Discover Materials

Research

Effect of Cu incorporation in silicate and modified borate bioglass materials for health applications: insights from synchrotron-based x-ray absorption spectroscopy

N. G. Imam[1,2] · Messaoud Harfouche[3] · A. M. Abdelghany[4] · Jan Ingo Flege[1]

Received: 1 November 2023 / Accepted: 23 July 2024
Published online: 29 July 2024

Abstract
This contribution investigates the effect of variable copper incorporation (*x = 0.2, 1.0, 2.0*, and *4.0*) in silicate (45 SiO_2, 24.5 CaO, 24.5 Na_2O, 6P_2O_5 *wt%*) and modified borate (45 B_2O_3, 24.5 CaO, 24.5 Na_2O, 6P_2O_5 *wt%*) bioglass materials to be used for bone bonding applications. X-ray absorption fine structure spectroscopy (XAFS) has been used to determine the oxidation states and local coordination structure of Cu atoms in silicate-based and borate-based glasses at the Cu K-edge (~ 8979 eV). The oxidation states of Cu atoms have been determined by near-edge XAFS (XANES) fingerprinting employing reference standard compounds of Cu. Cu (I) and Cu (II) XANES spectra of the standard reference compounds were linearly combined to fit the normalized μ(E) data of the collected XANES spectra using linear combination fitting (LCF approach). The obtained results prove that most of the silicate glass samples contain Cu_2O almost exclusively, while modified borate glass samples contain a significant mixture of Cu_2O and CuO phases. According to the literature, the remarkable coexistence of Cu_2O and CuO phases within the borate sample, particularly when *x* = 4, promotes the conversion process to allow the more facile formation of hydroxy carbonate apatite (HCA). The best fit structural parameters derived from extended-XAFS (EXAFS) fitting show that the ratio between Cu (I) and Cu (II) in borate glass agreed well with that extracted from XANES analysis. XANES and EXAFS conclude that borate glass with *x* = 4 is the most suitable composition for bone bonding applications.

Keywords Bioglass · Local coordination · Oxidation state · Silicate · Borate · Synchrotron radiation · Short-range order · XANES · LCF · EXAFS

1 Introduction

Silicate-based and borate-based bioglass of nominal compositions (45SiO_2, 24.5CaO, 24.5Na_2O, 6P_2O_5 *wt%*), (45B_2O_3, 24.5CaO, 24.5Na_2O, 6P_2O_5 *wt%*), respectively, containing variable Cu contents (*x*) in the range (0.2–4 additive) have attracted substantial interest due to their remarkable potential for use in health applications, e.g., in bone bonding [1, 2]. Thanks to the antimicrobial properties of copper, bioactive glasses containing Cu are useful in medical

✉ N. G. Imam, imamneam@b-tu.de; Messaoud Harfouche, messaoud.harfouche@sesame.org.jo; A. M. Abdelghany, a.m_abdelghany@yahoo.com; Jan Ingo Flege, flege@b-tu.de | [1]Applied Physics and Semiconductor Spectroscopy, Brandenburg University of Technology Cottbus-Senftenberg, Konrad-Zuse-Strasse 1, 03046 Cottbus, Germany. [2]Experimental Nuclear Physics Department (Solid State Physics Laboratory), Nuclear Research Center (NRC), Egyptian Atomic Energy Authority (EAEA), Cairo 13759, Egypt. [3]Synchrotron-Light for Experimental and Scientific Applications in the Middle East (SESAME), PO Box 7, Allan 19252, Jordan. [4]Spectroscopy Department, Physics Research Institute, National Research Center, 33 ElBehouth St., Dokki, Cairo 12311, Egypt.

applications where preventing infections is important [1–3]. When the glass comes in contact with bodily fluids, Cu ions are released, which can help inhibit the growth of bacteria and other microorganisms and increase the ability to promote tissue regeneration and its compatibility with biological systems [1–5]. Also, glass samples doped with Cu ions are used in wound healing applications as they have been shown to drastically boost blood vessel formation [6]. Borate glass is known for its unique behavior of fast degradation and formation of hydroxy carbonate apatite (HCA) and excluded with urine in addition to low cost and easy processability [1]. The reason for such a fast transformation was completely missed [1, 2]. The formation of hydroxyapatite (HA) or hydroxycarbonate apatite (HCA) on the surface of bioactive glasses and glass–ceramics is a crucial phenomenon that determines their bioactivity and bone-bonding ability [1–4]. Cu ions, in both their oxidation states, Cu (I) and Cu (II), can play a significant role in promoting HCA formation during the preparation of borate bioglass doped with Cu [7]. Further, Cu (II) ions can act as nucleation sites for the formation of HCA due to their ability to interact with the functional groups present in the surrounding environment since the presence of Cu (II) ions can enhance the formation of amorphous calcium phosphate (ACP) precursors, which serve as intermediates in the formation of HCA. Moreover, Cu (II) ions can also participate in the dissolution of the bioglass matrix, releasing calcium and phosphate ions, which are essential building blocks for HCA formation. Monovalent Cu (I) ions can also contribute to the formation of HCA, although their role may be less pronounced compared to Cu (II) ions. Cu (I) ions can participate in redox reactions, leading to the formation of reactive oxygen species (ROS), which can influence the local environment and promote the nucleation and growth of HCA. Cu (I) ions may also interact with functional groups on the bioglass surface, facilitating the adsorption and deposition of calcium and phosphate ions, leading to HCA formation [7–9].

To understand the role of Cu incorporation modifier silicate and borate glasses, X-ray absorption fine structure spectroscopy (XAFS) based on synchrotron radiation was used to explore the oxidation states as well as the local structure and coordination of Cu atoms [2–6]. Generally, to explain the specific physical and chemical properties of glassy materials, it is necessary to probe deeply into the structural properties of these materials; however, glassy materials are very often either amorphous or semi-crystalline materials characterized by the absence of long-range order [10]. The structural characterization of glassy materials has always been performed by probing the local atomic structural environment in the short-range order (1–5 Å) [11]. The challenge is then to investigate the effect and possibly establish a correlation between the short-range structure and the resulting different properties and applications of the bioglass materials. The high relevance of the structural investigations of glassy materials is not only due to the interest in explaining the physical and chemical features of these materials but also due to their wide spectrum of daily and potential applications [12]. Glass can be used, in medical applications as in bone bonding as mentioned above, in energy applications as in fuel cells, and in storing radioactive wastes [1, 2].

For more details, being a short-range local structural and selective elemental technique, XAFS is an ideal tool to structurally describe glass materials in the absence of long-range ordered structure [13]. XAFS provides valuable local structural information about oxidation states [14, 15], local coordination geometry, site-symmetry [16, 17], kind/type of neighbouring atoms, relative disorder, and angles between the central atom and nearest neighbours [18, 19]. Unlike some other techniques, XAFS can be used for probing either bulk or surface structure, by tuning the XAFS data collection mode [20]. Also, XAFS does not rely on bulk properties but is sensitive to atomic structure. XAFS operates at core-level X-ray absorption energies, corresponding to specific electron shells (typically, K and L shells). Also, due to its high sensitivity to subtle changes in the local environment, XAFS can detect variations in bond lengths, coordination numbers, and oxidation states corresponding to the change in composition/concentration of the central atom.

Generally, the XAFS spectrum consists of two energy regions: near-edge XAFS (also called X-ray absorption near-edge spectroscopy, XANES) that denotes the spectral region around the absorption edge, and extended XAFS (EXAFS) starting from around 100 eV after the absorption edge and extended up to more than 1000 eV. XANES probes the density of either the empty or partially filled electronic states by exciting the inner shell electron to those states [21]. As this electronic transition may only occur if it is allowed according to the dipole selection rule [(Δl) is ± 1], XANES probes the angular momentum of unoccupied electronic states.

On the other side, extended XAFS (EXAFS) is sensitive to the surrounding local structure of the absorber atom. The origin of the EXAFS signal is the interactions between the photoelectron excited from a deep core level of the absorbing atom by an incident X-ray photon with the electrostatic potentials of neighboring atoms. The presence of neighbouring atoms slightly perturbs the absorption probability, resulting in the oscillatory structure of the absorption coefficient μ(E) on top of smooth variations of the absorption probability μ0(E) that is unrelated to the sample structure. EXAFS delves deeper into the atomic structure, revealing details about neighbouring atoms and their bond distances [22, 23].

The aim of this work is to determine the oxidation states and local structural details of Cu atoms in order to probe the effect of boosting Cu oxide at the expense of B_2O_3 and SiO_4 in borate and silicate bioglass samples, respectively. The atomic local structure was studied by collecting Cu K-edge (8979 eV) XAFS spectra at beamline BM08-XAFS/XRF at the SESAME synchrotron [24, 25]. As stated before, for the healing process in bone bonding applications, the coexistence of Cu_2O and CuO within silicate or borate samples, with a significant *wt*% for each phase, will promote the conversion process to allow for a faster formation of HCA. Consequently, this work intends to find out the optimum Cu content (*x),* which forms a mixture of Cu (I) and Cu (II) with a significant *wt*% for both Cu phases.

2 Experimental procedure

2.1 Sample preparation

Silicate-based and borate-based bioglass of nominal compositions ($45SiO_2$, 24.5CaO, $24.5Na_2O$, $6P_2O_5$ *wt*%), ($45B_2O_3$, 24.5CaO, $24.5Na_2O$, $6P_2O_5$ *wt*%), respectively, containing variable Cu contents (*x*) in the range (0.2–4 additive) were synthesized using the melt quenching technique. Sample names and compositions are listed in Table 1. Analytical grade copper oxide was used as received, while calcium and sodium oxides were obtained from their carbonates. Ammonium dihydrogen phosphate and orthoboric acid were used as a source of phosphorus pentoxide and boron oxide, respectively. Weighed batches were sintered at 450 °C to remove carbonate, ammonia, and water. The oven temperature was gradually raised to 1200–1300 °C depending on the glass composition. The obtained melts were swirled many times to obtain a bubble-free sample. The melts were then poured into stainless steel moulds of the required dimensions.

To prepare the silicate and modified borate samples containing Cu for XAFS measurements, the calculated weight from each sample powder was homogeneously distributed into a reasonable amount of polyvinylpyrrolidone (PVP). The sample/PVP composites were pressed into pellets of 13 mm in diameter to allow the beam to probe a large area of the sample.

2.2 XAFS measurements and data collection

Using the BM08-XAFS/XRF beamline of the SESAME Synchrotron facility in Allan-Jordan [24, 25], Cu K-edge XAFS spectra were adequately acquired at ambient room temperature. SESAME is operated at 2.5 GeV with a maximum injection current of 250 mA [25]. The BM08-XAFS/XRF beamline has been constructed for providing hard X-rays in the range of (4.7–30) keV with high photon flux (10^9–10^{12} ph/s) and high beam stability and is dedicated to XAFS and XRF spectroscopic applications [24]. The beam spot size at the sample position is (1–20) mm horizontally, while it is (1–5) mm vertically. Double crystal monochromator equipped with Si (111) crystals is utilized, achieving an energy resolution ΔE of $\sim 2.4 \times 10^{-4}$ eV. Higher harmonics are effectively suppressed thanks to the Si-coated stripe of the collimating and focusing mirrors. Cu (0) metal foil was used for beamline energy calibration by assigning, through the derivative, the first inflection point of the tabulated K-edge of Cu foil (8979 eV). The sample XAFS spectra were collected in fluorescence mode (FL-mode) by using a silicon drift detector (SDD: Ketek) at 45 degrees with respect to the sample. The incident intensity (Io) was measured using a 150 mm ionization chamber (IC). The mixture of He, N_2, and Ar gas in the IC was optimized for a ~ 15% absorption of the total incident beam. XAFS data for reference samples (CuO, and Cu_2O) were collected in

Table 1 Silicate and modified borate bioglass compositions (in *wt*%) at different Cu content (*x*)

Sample	SiO_2	B_2O_3	CaO	Na_2O	P_2O_5	Copper oxide
BioSiGCu_0.2	44.8	–	24.5	24.5	6.00	0.20
BioSiGCu_1	44.0	–	24.5	24.5	6.00	1.00
BioSiGCu_2	43.0	–	24.5	24.5	6.00	2.00
BioSiGCu_4	41.0	–	24.5	24.5	6.00	4.00
BioBGCu_0.2	–	44.8	24.5	24.5	6.00	0.20
BioBGCu_1	–	44.0	24.5	24.5	6.00	1.00
BioBGCu_2	–	43.0	24.5	24.5	6.00	2.00
BioBGCu_4	–	41.0	24.5	24.5	6.00	4.00

transmission mode where the ionizing gas (He, N2, and Ar) in ionization chambers for sample transmission (I_1) and reference (I_2) was optimized for an absorption of 65% and 90%, respectively.

Our XAFS data were collected in the FL-mode with an energy step of 0.5 eV in the pre-edge region, 0.2 eV in the XANES region, and with a constant *k*-step of 0.03 $Å^{-1}$ in the EXAFS region. Four scans for each sample were recorded to improve the signal-to-noise ratio.

2.3 XAFS data processing and analysis

XAFS data were processed using standard procedures offered by the ATHENA program of the DEMETER software package [26, 27]. Accordingly, pre-edge absorption removal, background subtraction, normalization, energy conversion into *k*, weighing scheme, and Fourier filtering were performed. The threshold energy (E_0) was taken at the first inflection point of the absorption edge jump, also, initially, it was taken at the fraction of the edge step (at 0.5 of the normalized intensity). Also, the white-line maximum peak energy was determined. Linear combination fitting approach (LCF) was performed for each sample considering Cu_2O and CuO as constituent phases. Different XANES spectral features parameters were quantified from the XANES fingerprint spectra of different samples along with those of Cu standard compounds.

Fourier transforms (FT) of the k^2-weighted EXAFS function were taken by using a Hanning window. Artemis software package (Artemis program2 from DEMETER; version 0.9.26), was used for modeling and structural shell-fitting of the collected EXAFS oscillations. The analysis of the experimental EXAFS has been done by generating the theoretical model and fitting it to the collected data. The best fits of the EXAFS signal were done in R-space in the interval of 1.35–2.117 Å with Hanning window in the range of (3–9.6) $Å^{-1}$ of *k*. Only the first coordination shell was subject to the fitting since there is no clear spectral features for the next higher coordination shells due to/confirming the highly amorphous/disordered structure of the target glass samples.

Based on the results extracted from XANES fingerprint and LCF approach, the best fit structural parameters were extracted from EXAFS fitting by applying one structural model of Cu_2O in case of silicate samples and two structural models of both Cu_2O and CuO to fit modified borate samples. Considering the well-known EXAFS equation described in [23], the fit parameters included the amplitude reduction factor (S_0^2) and the correction to the difference in photoelectron energy (E_0) between the experimental data and theoretical model calculated using FEFF software package [27], which were set similarly for all scattering paths and fixed for all Cu content (x) to minimize the number of variable parameters and thus reduce the correlation among the fit parameters, also for a real comparison of the same samples with different *x*. While, interatomic distances (*R*) and variation in the interatomic distances or mean-square relative displacements (MSRDs), also known as Debye–Waller factors (σ^2), were refined to get the best-fit result. S_0^2 was determined to be ~0.97 by fitting the EXAFS data of the reference Cu foil with its well-known structure.

3 Results and discussion

3.1 XAFS study of silicate-based bioglass doped with Cu

Figure 1 exhibits the entire collected and normalized Cu K-edge XAFS spectra of bioglass of nominal composition ($45SiO_2$, 24.5CaO, $24.5Na_2O$, $6P_2O_5$ *wt%*) with variable Cu content (*x*) in the range of (0.2–4 additive). Figure 1 consists of two different XAFS parts; the first part is the near edge-XAFS or XANES, and the second part is the extended-XAFS or EXAFS. The two XAFS spectral parts are analyzed separately to extract complementary information about the electronic and local structure around Cu atoms. Consequently, to investigate the energy peak positions and spectral features of the pre-edge peak as well as the white-line of the XANES part, fingerprint XANES spectra of the samples are plotted along with those of Cu standard reference compounds as shown in Fig. 2.

The extracted spectral white-line peak position, absorption energies taken as the first inflection point of the rising absorption edge, and nominal oxidation states of Cu cations in the silicate glass matrix are listed in Table 2. From the first look at the pre-edge feature and based on the extracted data in Table 2, it is clear that the XANES spectra of silicate samples are quite similar to that of the Cu_2O standard reference. To confirm if the Cu cations in silicate glass form only a single phase of Cu_2O or if there are other (secondary) phases/species of Cu compounds such as Cu-metal and/or CuO present, a linear combination fitting (LCF) was performed for each sample XANES spectrum. This way, the contributing ratio of Cu (I), Cu (0), and/or Cu (II) phases in different silicate glass samples can be determined. The results of the best fits to the data are tabulated in Table 2. It is observed that all silicate glass samples contain mainly Cu_2O as shown in

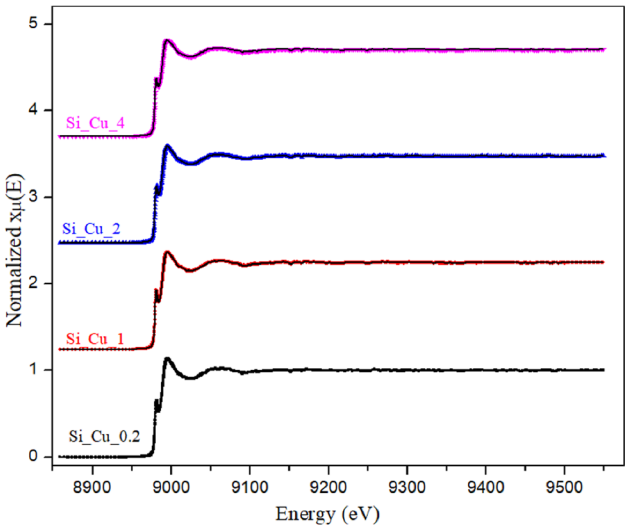

Fig. 1 Normalized Cu K-edge full XAFS spectra of Hench bioglass of nominal composition (45 SiO_2, 24.5 CaO, 24.5 Na_2O, 6P_2O_5 *wt*%) containing variable concentrations of copper oxide in the range (0.2–4 additive). All spectra are plotted with vertical offset, for clarity; xμ (E) is the total absorption, where x here is the thickness of the sample

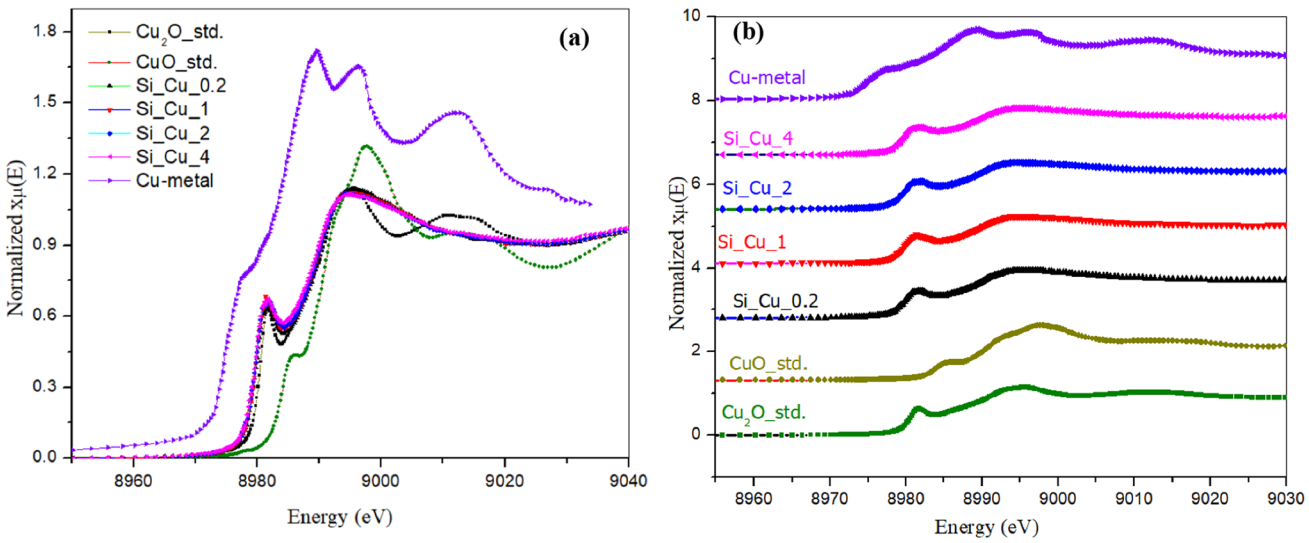

Fig. 2 Normalized fingerprint XANES spectra of the silicate glass samples along with those of different Cu standards without offset (**a**), and with vertical offset (**b**)

Fig. 3, which represents the best fit of silicate glass at $x = 4$ with Cu_2O standard reference. This result matches well with the published results by Gaur et al. [28].

EXAFS analysis was utilized to further explore the local structure around the Cu atoms. The Fourier transform (FT) is known as a complex function of bond length or distance R. The amplitude of FT is denoted by the real function χ(R); $|\chi(R)|$. The peak positions in χ(R) are related to bond lengths between the Cu and neighbouring atoms, whereas the height of each peak is proportional to the coordination number *N* [10, 11, and 14]. However, we cannot directly extract the bond lengths and coordination numbers from χ(R). Figure 4 displays Fourier Transform magnitudes of the extracted k^2-weighted EXAFS signals in silicate glass samples along with those of the Cu standard compounds (Cu (0), Cu (I) and Cu (II)) with y-offset (left) and without any offset (right), respectively.

It is clear that the silicate sample doped with Cu exhibits a decrease in FT amplitude upon increasing Cu content (x). Accordingly, the coordination number *N* decreases, which means that the structure disorder increases [15].

The fit of the EXAFS data of Cu doped silicate samples is exemplarily displayed in Fig. 5 for the Cu content of $x = 4$. The extracted fit parameters for all silicate glass samples are tabulated in Table 3. The first coordination shell is formed by bridging the Cu cation between two oxygen atoms, where two oxygen anions are located at a mean distance of an average of 1.85 ± 0.02 Å from the absorber atom (Cu). Closer examination reveals that the second peak in the FT plot is significantly broader than the corresponding peak of the Cu (I) standard, which indicates a lower degree of

Table 2 Spectral white-line position, absorption energy value, taken at the first inflection point of the absorption edge jump, and oxidation states

group (*x*)	White-line maximum peak position (eV) ± 0.33	E_0 (eV), ± 0.15	Oxidation state of Cu cations	*wt* % of Cu (I) ± 0.4%	*wt* % of Cu (II) ± 0.4%
Silicate glass					
"*x* = 0.2"	8995.44	8980.27	Cu (I)	100%	…….
"*x* = 1.0"	8995.52	8980.16	Cu (I)	100%	……
"*x* = 2.0"	8995.56	8980.15	Cu (I)	100%	……
"*x* = 4.0"	8995.95	8980.06	Cu (I)	100%	……
Modified borate glass					
"*x* = 0.2"	8996.53	8985.23	Cu (II) and Cu (I)	26.6%	73.4%
"*x* = 1.0"	8996.85	8985.26	Cu (II) and Cu (I)	26.2%	73.8%
"*x* = 2.0"	8996.54	8985.253	Cu (II) and Cu(I)	28.1%	71.9%
"*x* = 4.0"	8996.66	8984.22	Cu (II) and Cu (I)	38.6%	61.4%
Cu-foil	8993.43	8979	Cu (0)	….	……
Cu_2O	8995.54	8980.72	Cu (I)	100%	0%
CuO	8997.51	8988.15	Cu (II)	0%	100%

Also, best fit results of LCF for Cu K-edge XANES spectra of silicate and modified borate glass samples of different Cu content (*x*) along with those of Cu_2O and CuO reference standards

R-factor ~ 0.02 ± 0.006

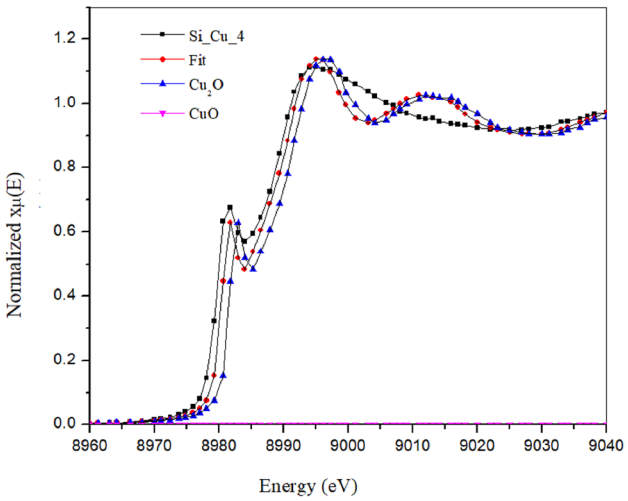

Fig. 3 Exemplary LCF of silicate glass at *x* = 4 with those of Cu_2O and CuO standard references

crystallinity of the copper oxide structure formed in silicate glass samples [29, 30]. Although glass materials are generally amorphous according to X-ray diffraction (XRD) analysis, XAFS (EXAFS) probes the local short-range structural order and may, as such, identify local bonding geometries as found in CuO or Cu_2O crystalline materials within an otherwise amorphous matrix.

It was reported that the incorporation of Cu (I) in glass materials by ion exchange or by introducing to the batch, a two-fold coordination state was proposed, while other researchers [31–33] assumed a six-fold coordination number. In this work, the guessed coordination number of Cu–O in the first coordination shell of silicate glass samples was set at 2. This value fitted well the EXAFS silicate data with that of Cu_2O standard and matched well with the fit performed by Tröger et al. [34].

3.2 XAFS study of the modified Borate-based bioglass doped with Cu

Figure 6 displays the normalized Cu K-edge full XAFS spectra of borate-based bioglass of nominal composition (45 B_2O_3, 24.5 CaO, 24.5 Na_2O, 6P_2O_5 *wt*%). The extracted spectral white-line peak position, absorption energies, and nominal

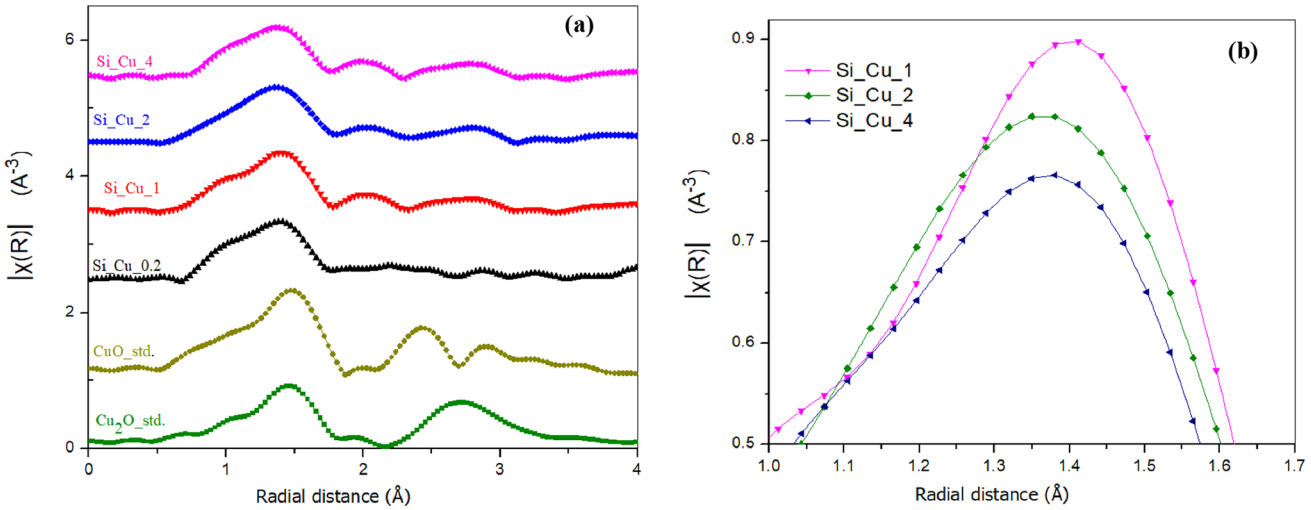

Fig. 4 k^2-weighted EXAFS oscillations of silicate glass samples along with those of Cu standard compounds; shifted vertically for clarity (**a**), and without vertical offset (**b**)

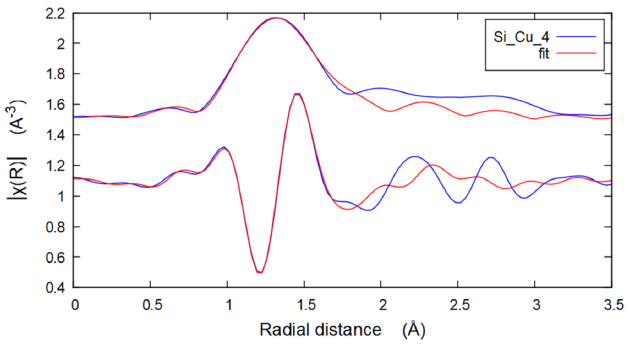

Fig. 5 Exemplary EXAFS fit obtained for the FT magnitude (upper) and the imaginary part (lower) of EXAFS signal at the Cu K-edge collected at $x = 4$ of silicate glass. The y-axis shows only the FT magnitude

Table 3 The best-fit local structural parameters of the first coordination shell around Cu ions (Cu–O) within silicate glass samples; $k = 2–9.6$ ($Å^{-1}$), R = 1–2.11 (Å), Hanning window, R-factor = 0.06 ± 0.02

Cu–O (1st shell) in Silicate glass fitted to Cu_2O model Cu content (x)	*R_Cu₂O(Å)* *Cu–O*
$\Delta E = -6 \pm 2$ eV, $S_0^2 = 0.97$, N = 2, $\sigma^2(Å^2) = 0.005 \pm 0.002$	
BioSiGCu_0.2	1.78 ± 0.03
BioSiGCu_1	1.88 ± 0.02
BioSiGCu_2	1.88 ± 0.04
BioSiGCu_4	1.89 ± 0.02
Cu_2O_Stand	1.83 ± 0.04

oxidation states of Cu cations in the borate glass matrix are shown in Table 2. It is observed from Table 2 that the white-line peak position (8996 eV) and the absorption edge (8985 eV) are diagnostics of mainly Cu (II) compounds, as reported in [31].

Figure 7 shows XANES fingerprints of different borate glass samples along with those of Cu (0), Cu (I), and Cu (II) standard XANES spectra. XANES analysis shows that there is a small shoulder around 8879.5 eV, indicating the existence of the Cu (II) phase. On the other hand, all XANES spectral features and parameters in Table 2 show that the Cu cations in borate glass samples may take multiple oxidation states, i.e., Cu (II), Cu (I), and/or Cu (0) [34].

Figure 8 represents LCF model example at $x = 4$ of borate glass samples. It is observed that the different Cu cations with different oxidation states and their contribution within borate glass samples can be distinguished. The best fit to the data from the LCF approach are presented in Table 2.

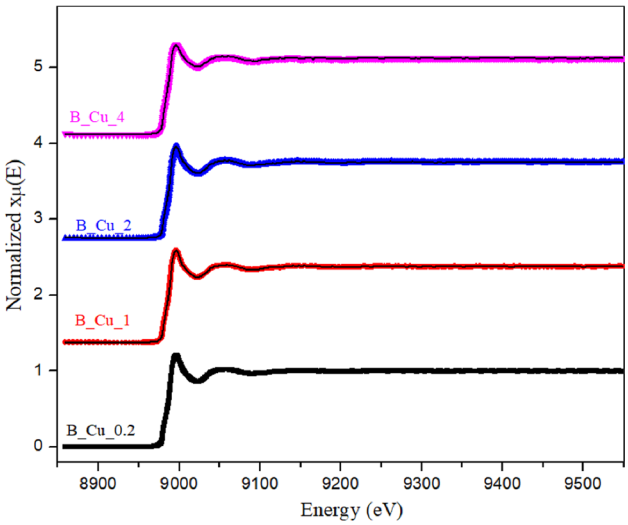

Fig. 6 Normalized Cu K-edge full XAFS spectra of Hench bioglass of nominal composition (45 B_2O_3, 24.5 CaO, 24.5 Na_2O, 6P_2O_5 *wt%*) with vertical offset

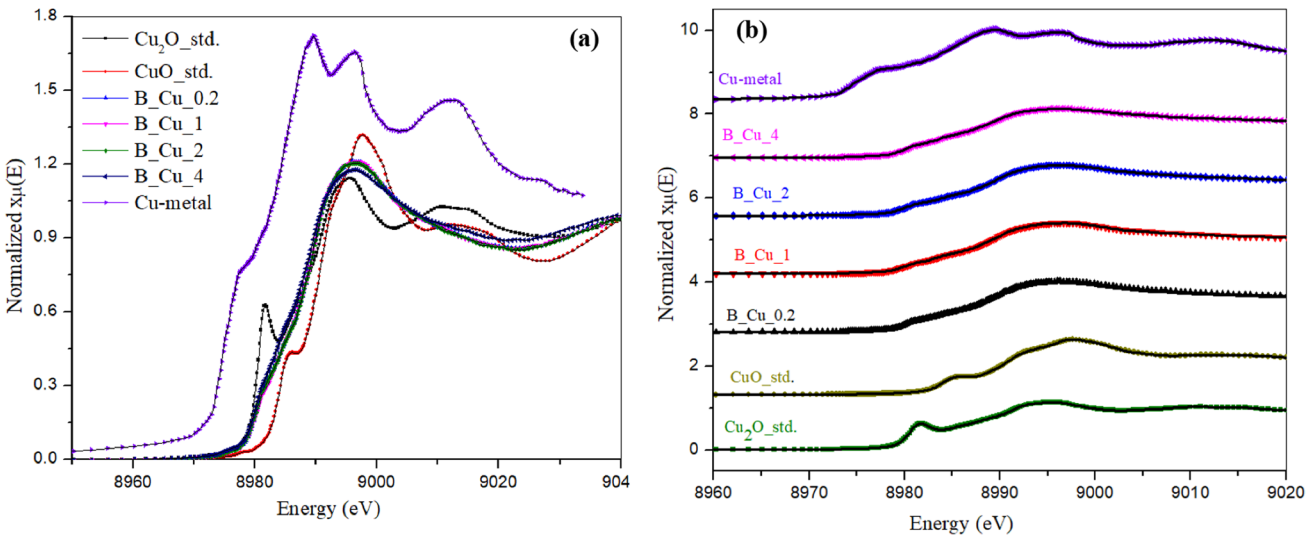

Fig. 7 Normalized Cu K-edge XANES spectra of Hench bioglass of nominal composition (45 B_2O_3, 24.5 CaO, 24.5 Na_2O, 6P_2O_5 *wt%*), along with those of Cu_2O and CuO reference standard compounds, without offset (**a**) and with vertical offset (**b**)

It is clearly shown that XANES spectral features and parameters of the modified borate glass samples are quite different from those obtained from the silicate glass samples. In order to confirm the difference between XANES spectral features of silicate and borate samples, XANES spectra of borate and silicate glasses at $x = 2$, (as an example), compared with those of XANES spectra of Cu standard compounds are shown in Fig. 9. For comparison, the borate glass XANES spectrum shows a shoulder at the absorption edge and an intense white line. While, the silicate glass samples show a characteristic sharp absorption peak without any pre-absorption peak like Cu (I) species due to its d^{10} electronic configuration, and thus lack of a classic $1s \rightarrow 3d$ pre-edge transition.

Figure 10 shows the FT magnitudes of the k^2-weighted EXAFS signals of different borate glass samples (45 B_2O_3, 24.5 CaO, 24.5 Na_2O, 6P_2O_5 *wt%*). The FT features of the modified borates can be modelled by considering the two structural models of the Cu (I) and Cu (II) standard references with different *wt%* (in the first coordination shell), as shown in Fig. 11. However, at longer distances, it seems that the local structure of borate glass samples has a higher disorder beyond the first coordination shell. It is clear that there is a remarkable reduction in FT amplitude with corresponding enhancement in the amount of Cu species. However, the samples of $x = 0.2$ and $x = 1$ present similarities in FT amplitude as well as the interatomic distance values. This result matches well with the LCF results Table 2. The reduction in the FT amplitude with changing Cu content is related to the evolution of Cu_2O/CuO ratio, which leads to boosting the disorder parameter, which, in turn, leads to a lowering in coordination number *N*. Furthermore, the highest next coordination shells of Cu–O

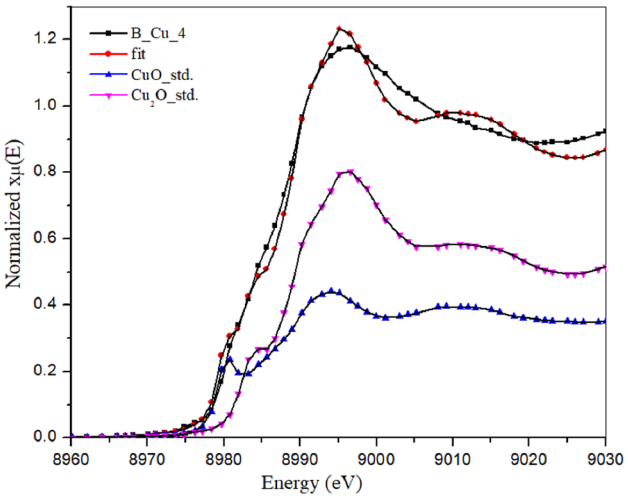

Fig. 8 Best fit results of LCF for Cu K-edge XANES spectrum of borate bioglass at $x=4$ (as an example), along with those of Cu_2O and CuO standards; LCF fitting in the range from −20eV to +20 eV around the absorption edge

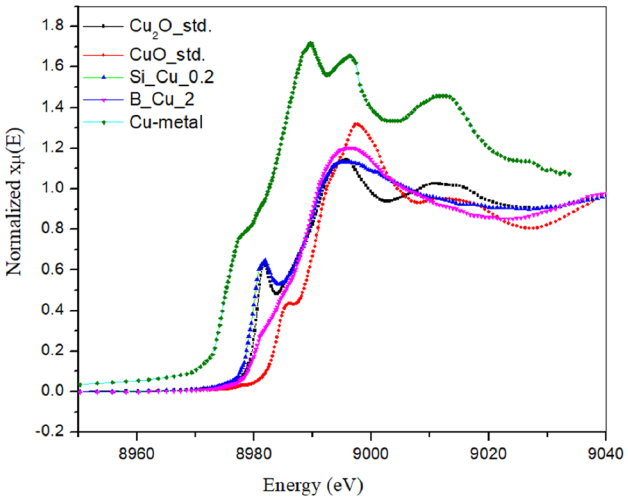

Fig. 9 Comparison between XANES spectra of borate and silicate bioglass at 2% of Cu (as an example), along with those of Cu standard compounds

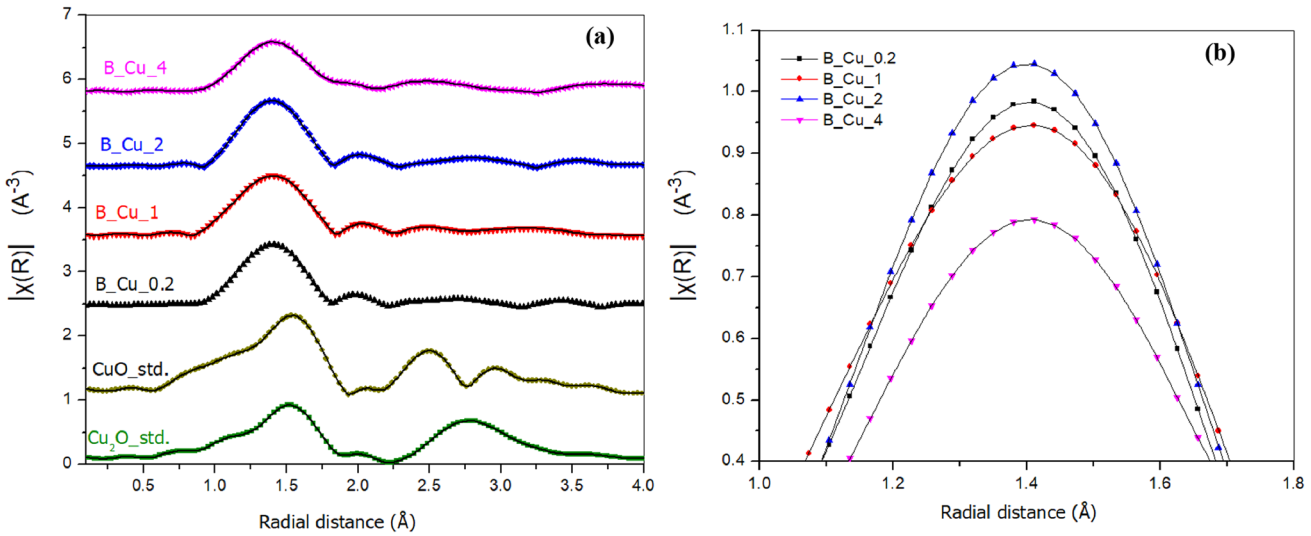

Fig. 10 k^2-weighted EXAFS signals of modified borate bioglass samples along with those of Cu standard compounds; shifted and arranged vertically (**a**) and without y-offset (**b**)

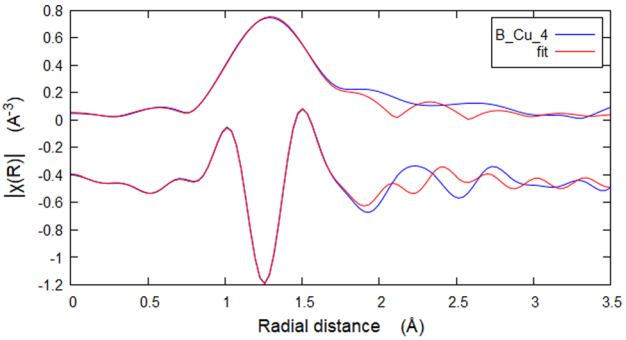

Fig. 11 EXAFS fit obtained for FT of EXAFS signal at Cu K-edge collected at x = 4 (as an example), of modified borate bioglass

and Cu–Cu bonds are not as well seen as those for Cu_2O and CuO standards, providing a lower degree of crystallinity of Cu-doped modified borate glass systems [35].

Table 4 clearly illustrates the fitted R-distances of the samples of $x = 0.2$, 1, and 2 are very close to each other, containing 2 (Cu–O) distances at 1.89 ± **0.02** Å, plus 6 (Cu–O) distances at 1.94 ± **0.02** Å. However, the sample of $x = 4$ shows a small change in the R-distances; 2 (Cu–O) distances at 1.91 ± **0.02** Å, plus 6 (Cu–O) distances at 1.95 ± **0.02** Å.

In addition, Table 4 shows that the disorder parameter of Cu–O distance in the CuO phase is higher than that of Cu_2O.

It was reported [36–39] that the structural coordination of CuO in various glass compositions was an elongated octahedron <CuO_6>, which agrees well with our fitting results of the coordination number of Cu(II) in the modified borate glass for the first coordination shell.

Finally, the obtained findings shed light on the difference in the bioactivity of both borate and silicate matrices. It is known that borate glass is an amorphous/disorder material; the coexistence of CuO and Cu_2O phases confirms the increase in the degree of disorder as extracted from EXAFS fitting. Modified borate glasses are known to be more efficient than that of their silicate partner (45S5 Hench Bioglass) resulting from the ease of conversion to their respective hydroxyapatite compartment and their low melting temperatures. The local structure of the matrices or the ease of degradation may be the result of such variation of the copper coordination within the glass matrix and reliability to be used in different medical applications, including hard tissue replacement [40–43].

4 Conclusions

This paper contributes to explaining the difference in the bioactivity of both borate and silicate matrices by following the short-range local structural change around the Cu atoms upon altering the Cu content (x), using XAFS. Near-edge XAFS (XANES) analysis confirms the formation of mixtures of Cu_2O and CuO within the modified borate bioglass, while the silicate glass samples contain mainly Cu_2O. According to the literature, a reasonable coexistence of both types of Cu ions has been proven to promote the formation of HCA, i.e., a suitable mixture of Cu(I) and (II) ions is needed for applications in bone bonding applications. Of our samples, the one with $x = 4$ seems the best. The XANES and EXAFS analyses yield consistent results regarding the relative amounts of Cu_2O and CuO phases. Lastly, XAFS offers unique advantages for this type of functional materials analysis, including element specificity, short-range sensitivity, and the ability to explore

Table 4 The best-fit local structural parameters of the first coordination shell around Cu ions within the modified borate glasses (Cu–O); $k = 2$–9.6 (Å^{-1}), R = 1–2.11 (Å), Hanning window

Cu–O (1st Shell) in borate glass fitted to Cu_2O and CuO models Cu content (x)	R_Cu_2O (Å)	R_CuO (Å)	wt% of Cu_2O	wt% of CuO
ΔE = −6 ± 2 eV, $S_0^2 = 0.97$, N = 2, σ^2_Cu_2O (Å^2) = 0.003 ± 0.001, σ^2_CuO (Å^2) = 0.015 ± 0.003				
BioBGCu_0.2	1.89 ± 0.02	1.94 ± 0.02	26%	74%
BioBGCu_1	1.89 ± 0.02	1.94 ± 0.02	26%	74%
BioBGCu_2	1.89 ± 0.02	1.94 ± 0.02	28%	72%
BioBGCu_4	1.91 ± 0.02	1.95 ± 0.02	35.6%	64.4%
Cu_2O_Stand	1.83 ± 0.02	……	100%	0%
CuO_Stand	…….	1.96 ± 0.02	0%	100%

local structures and oxidation states. As XANES/EXAFS analysis can deliver such chemical and structural information, we may conclude that these methods are well suited to shed light on the materials used in bone bonding applications.

Acknowledgements The Synchrotron radiation of XAFS measurements were performed at Synchrotron-light for Experimental Science and Applications in the Middle East (SESAME), Jordan. The authors acknowledge support by SESAME and BM08-XAFS/XRF Beamline staff.

Author contributions N. G. Imam, A. M. Abdelghany, and Messaoud Harfouche collected the XAFS Data at SESAME synchrotron. The bio-glass materials were synthesized by A. M. Abdelghany. N.G. Imam did XAFS data analyses and fitting. N.G. Imam interpreted the results and wrote the first draft of the manuscript. Jan Ingo Flege is supervision, revised the final form of the paper and contributed in the discussion of the presented results. Also, professor Flege rewrote the discussion of this manuscript.

Data availability The authors confirm that the data supporting the findings of this study are available within the article and there is no supplementary information. However, the original collected data are available from the corresponding author upon reasonable request.

Declarations

Ethics approval and consent to participate No ethical approval was required for this research as it did not involve human tissue or any other parts of living organisms.

Competing interests The authors declare that they have no conflict of interest.

References

1. El-Batal FH, Khalil EM, Hamdy YM, Zidan HM, Aziz MS, Abdelghany AM. FTIR spectral analysis of corrosion mechanisms in soda lime silica glasses doped with transition metal oxides. SILICON. 2010;2:41.
2. Diab HM, Abdelghany AM, Hafez HS. Dosimetric behavior of modified borate bioglass containing copper for low photon dose measurements using luminescence characteristics. J Mater Sci Mater Electron. 2020;31:20452.
3. Abdelghany AM, Diab HM, Madbouly AM, Ezz-ElDin FM. Inspection of radiation shielding proficiency and effect of gamma-ray on ESR and thermal characteristics of copper oxide modified borate bioglasses. J Inorg Organomet Polym Mater. 2022;32:3204.
4. Choe YE, Kim YJ, Jeon SJ, Ahn JY, Park JH, Dashnyam K, et al. Investigating the mechanophysical and biological characteristics of therapeutic dental cement incorporating copper doped bioglass nanoparticles. Dent Mater. 2022;38:363.
5. Stähli C, James-Bhasin M, Hoppe A, Boccaccini AR, Nazhat SN. Effect of ion release from Cu-doped 45S5 Bioglass® on 3D endothelial cell morphogenesis. Acta Biomater. 2015;19:15.
6. Rivera LR, Cochis A, Biser S, Canciani E, Ferraris S, Rimondini L, et al. Antibacterial, pro-angiogenic and pro-osteointegrative zein-bioactive glass/copper based coatings for implantable stainless steel aimed at bone healing. Bioactive Mater. 2021;6:1479.
7. Terczyńska-Madej A, Cholewa-Kowalska K, Łączka M. Coordination and valence state of transition metal ions in alkali-borate glasses. Opt Mater. 2011;33:1984.
8. Dyar MD. A review of Mössbauer data on inorganic glasses: the effects of composition on iron valency and coordination. Am Miner. 1985;70:304.
9. Ghazy AR, Elmowafy BM, Abdelghany AM, Meaz TM, Ghazy R, Ramadan RM. Structural, optical, and cytotoxicity studies of laser irradiated ZnO doped borate bioactive glasses. Sci Rep. 2023;13:7292.
10. De Sousa EMB, Porto AO, Schilling PJ, Alves MCM, Mohallem NDS. Study of the structural evolution of copper-doped porous silica gels. Phys Chem Solids. 2000;61:853.
11. Onodera Y, Kohara S, Salmon PS, Hirata A, Nishiyama N, Kitani S, Zeidler A, Shiga M, Masuno A, Inoue H, Tahara S, Polidori A, Fischer HE, Mori T, Kojima S, Kawaji H, Kolesnikov AI, Stone MB, Tucker MG, Donnell MT, Hannon AC, Hiraoka Y, Obayashi I, Nakamura T, Akola J, Fujii Y, Ohara K, Taniguchi T, Sakata O. Structure and properties of densified silica glass: characterizing the order within disorder. NPG Asia Mater 2020;12:85. https://doi.org/10.1038/s41427-020-00262-z.
12. Imam NG, AbouHasswa M, Aquilanti G, El Dek SI, Okasha N, Al Shahawy AAG. Influence of polyethylene glycol on the physical properties of Co0. 2Fe2. 8O4 nanoparticles used as MRI contrast agent; synchrotron radiation Fe K-edge XAFS. J Mater Res Technol. 2021;15:4130.
13. Mastelaro VR, Zanotto ED. X-ray absorption fine structure (XAFS) studies of oxide glasses—a 45-year overview. Materials (Basel). 2018;28:204.
14. Klepka MT, Wolska A, Drzewiecka-Antonik A, Rejmak P, Hatada K, Aquilanti G. XAFS study of bioactive Cu (II) complexes of 7-hydroxycoumarin derivatives in organic solvents. Chem Phys Lett. 2017;673:113.

15. Arman MM, Imam NG, Portales RL, El-Dek SI. Synchrotron radiation X-ray absorption fine structure and magnetization improvement of A-site Ce3+ doped LaFeO3. J Magn Magn Mater. 2021;513: 167097.
16. Imam NG, Aquilanti G, Azab AA, Ali SE. Correlation between structural asymmetry and magnetization in Bi-doped LaFeO 3 perovskite: a combined XRD and synchrotron radiation XAS study. Mater Sci Mater Electron. 2021;32:3361.
17. Imam NG, AbouHasswa M, Okasha N. Synchrotron X-ray absorption fine structure study and dielectric performance of Li0. 5Fe2. 5O4/BaTiO3 multiferroic. Mater Sci Mater Electron. 2021;32:21492.
18. Imam NG, AbouHasswa M, Ali AI, Okasha N. Optimization of magnetic properties of BaTiO3/Li0. 5Fe2. 5O4 multiferroics prepared via modified low-temperature combustion. Mater Sci Mater Electron. 2022;33:7945.
19. Elyamny S, Imam NG, Aquilanti G, Cabrera H, Kashyout AB. Thermal transport properties for unveiling the mechanism of BiSbTe alloys in thermoelectric generation: a glance from synchrotron radiation Bi L3-XAFS. J Mater Res Technol. 2022;18:2261.
20. Imam NG, Elyamny S, Aquilanti G, Pollastri S, Gigli L, Kashyout AE. Comprehensive study of nanostructured Bi 2 Te 3 thermoelectric materials–insights from synchrotron radiation XRD, XAFS, and XRF techniques. RSC Adv. 2024;14:1875. https://doi.org/10.1039/d3ra06731a.
21. D'Acapito F, Mobilio S, Regnard JR, Cattaruzza E, Gonella F, Mazzoldi P. The local atomic order and the valence state of Cu in Cu-implanted soda-lime glasses. J Non-Cryst Sol. 1998;232:364.
22. Fukumi K, Chayahara A, Kadono K, Kageyama H, Akai T, Kitamura N, et al. Structural investigation on implanted copper ions in silica glass by XAFS spectroscopy. J Non-Cryst Sol. 1998;238:143.
23. Bunker G. Introduction to XAFS. New York: Cambridge University Press; 2010.
24. Imam NG, Harfouche M, Azab AA, Solyman S. Coupling between γ-irradiation and synchrotron-radiation-based XAFS techniques for studying Mn-doped ZnO nanoparticles. J Synchrotron Rad. 2022;29:1187.
25. Harfouche M, Abdellatief M, Momani Y, Abbadi A, Najdawi M, Alzu'bi M, et al. Emergence of the first XAFS/XRF beamline in the Middle East: providing studies of elements and their atomic/electronic structure in pluridisciplinary research fields. J Synchrotron Rad. 2022;29:1107.
26. Bourke JD, Chantler CT, Joly Y. FDMX: extended X-ray absorption fine structure calculations using the finite difference method. J Synchrotron Rad. 2016;23:551.
27. Ravel B, Newville M. ATHENA, ARTEMIS, HEPHAESTUS: data analysis for X-ray absorption spectroscopy using IFEFFIT. J Synchrotron Rad. 2005;12:537.
28. Gaur A, Shrivastava BD, Joshi SK. Copper K-edge XANES of Cu (I) and Cu (II) oxide mixtures. J Phys Conf Ser. 2009;190: 012084.
29. Lee J, Yano T, Shibata S, Nukui A, Yamane M. EXAFS study on the local environment of Cu+ ions in glasses of the Cu2O–Na2O–Al2O3–SiO2 system prepared by Cu+/Na+ ion exchange. J Non-Cryst Sol. 2000;277:155.
30. Maurizio C, D'Acapito F, Benfatto M, Mobilio S, Cattaruzza E, Gonella F. Local coordination geometry around Cu and Cu ions in silicate glasses: an X-ray absorption near edge structure investigation. Eur Phys B Condens Matter Complex Syst. 2000;14:211.
31. Kamiya K, Okasaka K, Wada M, Nasu H, Yoko T. EXAFS study on the local environment around copper in low thermal expansion copper aluminosilicate glasses. J Am Ceram Soc. 1992;75:477.
32. Kaufmann J, Rüssel C. Thermodynamics of the Cu+/Cu2+-redox equilibrium in soda-silicate and soda-lime-silicate melts. J Non-Cryst Solids. 2009;355:531.
33. Maurizio C, D'Acapito F, Sada C, Cattaruzza E, Gonella F, Battaglin G. Site of transition metal ions in ion-exchanged metal-doped glasses. Mater Sci Eng B. 2008;149:171.
34. Tröger L, Yokoyama T, Arvanitis D, Lederer T, Tischer M, Baberschke K. Determination of bond lengths, atomic mean-square relative displacements, and local thermal expansion by means of soft-x-ray photoabsorption. Phys Rev B. 1994;49:888.
35. Bäck LG. Electronic spectra and molar extinction coefficient of Cu2+ in mixed alkali–alkaline earth–silica glasses. Phys Chem Glas Eur J Glass Sci Technol B. 2015;56:8.
36. Monged MHE, Imam NG, Aquilanti G, Pollastri S, Rashad AM, Osan J. Heavy metals concentrations and speciation of Pb and Ni in airborne particulate matter over two residential sites in Greater Cairo–reflection from synchrotron radiation. J Synchrotron Rad. 2022;29:765.
37. Nadji A, Abu Ghannam S, Hoorani HR, Qazi Z, Saleh I, Gournay JF et al. The SESAME Project, Proceedings of ICALEPCS2011, Grenoble, France; 2011
38. Rao TGVM, Kumar AR, Chakravarthi CK, Reddy MR, Veeraiah N. Spectroscopical splitting of Cu ion energy levels in magnesium lead fluoro silicate glasses. Phys B Condens Matter. 2012;407:593.
39. Kau LS, Spira-Solomon DJ, Penner-Hahn JE, Hodgson KO, Solomon EI. X-ray absorption edge determination of the oxidation state and coordination number of copper. Application to the type 3 site in Rhus vernicifera laccase and its reaction with oxygen. J Am Chem Soc. 1987;109:6433.
40. Kristiansen T, Mathisen K, Einarsrud M, Bjørgen M, Nicholson DG. Single-site copper by incorporation in ambient pressure dried silica aerogel and xerogel systems: an X-ray absorption spectroscopy study. J Phys Chem C. 2011;115:19260.
41. Pickup DM, Ahmed I, FitzGerald V, Moss RM, Wetherall KM, Knowles JC, et al. X-ray absorption spectroscopy and high-energy XRD study of the local environment of copper in antibacterial copper-releasing degradable phosphate glasses. J Non-Cryst Solids. 2006;352:3080.
42. Samir A, Hassan MA, Abokhadra A, et al. Characterization of borate glasses doped with copper oxide for optical application. Opt Quant Electron. 2019;51:123.
43. ElBatal HA, Abdelghany AM, Goneim NA, ElBatal FH. Effect of 3d-transition metal doping on the shielding behavior of barium borate glasses: a spectroscopic study. Spectrochim Acta Part A Mol Biomol Spectrosc. 2014;133:534–41.